

Design and Stiffness Analysis of 12 DoF Poppy-inspired Humanoid

Dmitry Popov, Alexandr Klimchik and Ilya Afanasyev

Institute of Robotics, Innopolis University, Universitetskaya Str. 1, Innopolis, Russia

Keywords: Stiffness Modeling, Human Mechatronics, Motion Control Systems, Robot Kinematics.

Abstract: This paper presents a low-cost anthropomorphic robot, considering its design, simulation, manufacturing and experiments. The robot design was inspired by open source Poppy Humanoid project and enhanced up to 12 DoF lower limb structure, providing additional capability to develop more natural, fast and stable biped robot walking. The current robot design has a non-spherical hip joint, that does not allow to use an analytical solution for the inverse kinematics, therefore another hybrid solution was presented. Problem of robot joint's compliance was addressed using virtual joint method for stiffness modeling with further compensation of elastic deflections caused by the robot links weight. Finally, we modeled robot's lower-part in V-REP simulator, manufactured its prototype using 3D printing technology, and implemented ZMP preview control, providing experiments with demonstration of stable biped locomotion.

1 INTRODUCTION

The progress in creation of highly specialized robotic systems contributes to automation of different everyday life aspects that can partially or fully replace humans in the future in some routine activities. The development of androids is one of the most relevant solution for successful robot operations in human environment with enhanced functionality. These robots usually resemble human beings in appearance and/or internal construction, having the similar body shape structure and walking principles. One of the most important part of an anthropomorphic robot is a pelvis with the lower limbs, which form the lower-part body. During last decades, robotics community has proposed some successful models of biped robots with similar lower limb structure with 6 Degree of Freedom (DoF) per leg, having 3 DoF hip, 1 DoF knee, and 2 DoF ankle. Thus, there are some well-known human-size androids like Honda ASIMO (Sakagami et al., 2002), WABIAN from Waseda University (Yamaguchi et al., 1999), Boston Dynamics Atlas (not a commercially available model), Pal Robotics Reem-C (Ferro and Marchionni, 2014), Android Technics AR-600 (Khusainov et al., 2015), etc. But for small-size robots the most popular models are ROBOTIS Darwin (Ha et al., 2011), Aldebaran Robotics Nao (Gouaillier et al., 2009) and Poppy Humanoid¹ with

5 DoF leg (Lapeyre et al., 2013b).

Stiffness modeling in robotics is considered for industrial manipulators, where problem of end-effector precise positioning under external and internal load are critical (Pashkevich et al., 2011). In humanoid robots accurate positioning is not always necessary, but with high compliance in links or joints, deflections caused by payload or link weights can affect robot stability. Therefore those deflections should be considered and compensated as possible.

Our goals in this paper are:

1. Adapt Poppy-like robot to new mechanical structure with 6 DoF lower limbs, which are able to support robot's upper-part (including a torso, hands, a head, sensors and a possible payload).
2. Implement stiffness model of the robot.
3. Develop software for fast, stable robot walking that also considers robot joints compliances and successfully eliminates them.
4. Reduce the robot production cost using hobby servomotors, inexpensive fabrication methods and cost-efficient electronics components.

The rest of the paper is organized as follows. Section 2 presents the robot design. Section 3 considers robot lower body's kinematics analysis including forward, inverse kinematic problem and robot workspace. Section 4 describes stiffness model. Section 5 includes trajectory planning and compensation.

¹Open source Poppy Humanoid project, www.poppy-project.org

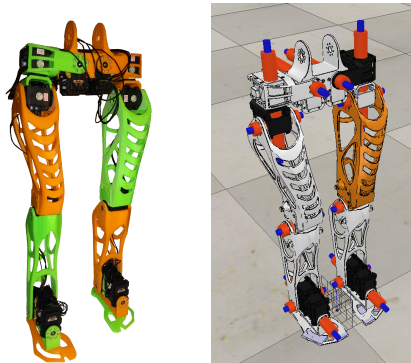
Finally, we conclude in section 6 with discussion on future work.

2 ROBOT DESIGN

The main feature of two-legged robot platform is the ability to walk. Therefore, the human body has been taken as a reference of the most advanced two-legged mechanism. In general human leg has dozen of DoF, but in case of bipedal walking, leg motions can be approximated with 6 DoF, three in the sagittal plane (ankle, knee, hip), one in the horizontal plane (hip) and two in the frontal plane (hip, ankle). Existing open source project Poppy has only 5 DoF per leg, 3 DoF in hip, 1 DoF in knee, and 1 DoF in ankle. In order to use standard 6 DoF approximation, addition DoF was added in the ankle. Usage of expensive Robotis Dynamixel MX-28, MX-64 is another problem of Poppy. To reduce overall cost of the robot, we propose to use more cheaper SpringRC SR-518 servomotors with 2 Nm torque and RS485 bus connection. Mounting places were also altered in order to fit this new motors.

Since human thigh bones are inclined by 6-7 degrees, it was also implemented by (Lapeyre et al., 2013a) in Poppy robot and our robot limb design. It allows to reduce falling speed and decrease the lateral motion of torso for single support phase and double support phase respectively. In order to make robot construction lighter and stiffer, we used mesh structure for thigh and shin.

Usually, most biped robots have unproportionally big foot. It is required in order to increase passive stability with increased support polygon. In our project, the foot size is proportional to human foot, thus providing additional difficulties to stabilization algorithms, but at the same time increasing robot mobility (Lapeyre et al., 2014).



(a) 3D printed prototype. (b) Model in V-REP.

Figure 1: Bipedal robot.

Table 1: Robot model joint range of motion.

Joint	Human (deg.)	Robot (deg.)
Hip Y	-30 to 45	-25 to 45
Hip Z	-45 to 50	-40 to 60
Hip X	-15 to 130	-60 to 100
Knee X	-10 to 155	-6 to 112
Ankle X	-20 to 50	-35 to 30
Ankle Y	-30 to 60	-35 to 35

Table 2: Robot model mass parameters.

Name	Mass (kg)	Mass Poppy (kg)
Thigh	0.226	0.239
Shin	0.124	0.108
Foot	0.116	0.047
Total	1.21	1.14

Table 3: Robot model size parameters.

Name	Size (mm)	Size Poppy (mm)
Thigh	181	181
Shin	178	177
Foot	129 x 63	145 x 50
Total	129 x 200 x 500	145 x 187 x 495

According to Table 1, robot leg's motion range is close to human, excepting joints with rotation around X axis. Their range is enough for walking, but can limit robot maneuverability for other activities. The limitations on joint motion range will be considered in Section 5.

In order to specify requirements to the robot hardware part, the combination of Dassault Systemes SolidWorks CAD tool and robot simulator Coppelia Robotics V-REP were used (Rohmer et al., 2013).

Robot prototype was manufactured using Fused Deposition Modeling (FDM) technique with Acrylonitrile butadiene styrene (ABS) polymer. It allows to reproduce robot mechanical part on every low-cost 3D printer.

Manufactured prototype and robot model in simulation environment are shown in Figure 1a and 1b correspondingly. Table 2 and 3 shows proposed robot mass and size parameters in comparison with lower half of Poppy robot. Total mass and size parameters remains the same, despite additional servomotor in ankle joint (6th DoF).

Table 4: Robot model mDH parameters.

θ_n	d_n , mm	a_{n-1} , mm	α_{n-1} , rad	Offset
q1	0	19 (y0)	$\pi/2$	0
q2	47 (z2)	52 (y1)	$\pi/2$	$\pi/2$
q3	0	0	$\pi/2$	$\pi/2$
q4	-23 (-y3)	181 (z3)	0	0
q5	0	178 (z4)	0	0
q6	0	0	$\pi/2$	0

3 KINEMATICS MODELING

3.1 Forward Kinematics

Forward or direct kinematics is the task of determining the position and orientation of the end-effector by giving configuration of the robot. The robot can be modeled as a kinematic chain of 7 links connected by 6 joints. The base frame of the robot located in the center of the waist. The local frames are assigned to joints, according to modified Denavit-Hartenberg (mDH) convention presented in (Craig, 2005). Table 4 shows robot mDH parameters. Since the right and left leg are identical, kinematics only for one leg will be considered.

$$TF = T0 * T1 * T2 * T3 * T4 * T5 * T6 * T7 = \begin{bmatrix} r11 & r12 & r13 & Tx \\ r21 & r22 & r23 & Ty \\ r31 & r32 & r33 & Tz \\ 0 & 0 & 0 & 1 \end{bmatrix} \quad (1)$$

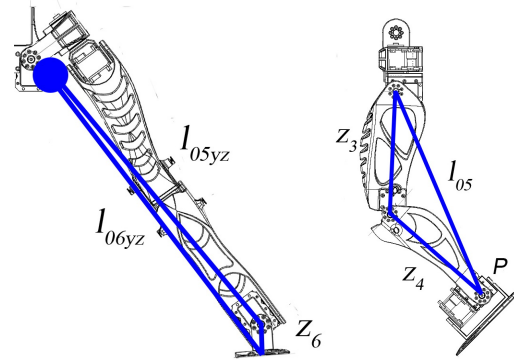
Final transformation matrix TF from the base to the end-effector can be obtained by multiplying transformational matrices of all joints (1).

3.2 Inverse Kinematics Problem

The purpose of solving the inverse kinematics (IK) is to find the angle of each joint for a known foot position and orientation. IK can be solved in two different ways: analytically and numerically. Analytical solution for 6 DoF serial manipulator can be hard to obtain directly or geometrically like in chapter 1 (Siciliano and Khatib, 2008), so different advanced techniques like Pieper method are usually used.

3.2.1 Analytical Solution

For solving IK with (Pieper, 1968) method serial manipulator should have 3 joints with consecutive axes



(a) Frontal plane. (b) Sagittal plane.

Figure 2: Robot leg.

intersecting at one point. Its not possible to use it for the considered robot. Therefore, let us consider another, similar modification, with spherical joint in the hip.

In order to simplify inverse kinematics, it is possible to find a geometrical solution for frontal (Figure 2a) and sagittal (Figure 2b) planes separately. Intermediate steps of finding inverse kinematics solution can be found in appendix of this paper.

$$q1 = \sin^{-1}(r32 \cdot \cos(q6) - r33 \cdot \sin(q6)) \quad (2)$$

$$q2 = \text{atan2} \left(\frac{r12 \cdot \cos(q6) - r13 \cdot \sin(q6)}{r22 \cdot \cos(q6) - r23 \cdot \sin(q6)}, \frac{-\cos(q1)}{\cos(q1)} \right) \quad (3)$$

$$q3 = \text{atan2}(-z4 \cdot \sin(q4) \cdot A + (z3 + z4 \cdot \cos(q4)) \cdot B, z4 \cdot \sin(q4) \cdot B + (z3 + z4 \cdot \cos(q4)) \cdot A) \quad (4)$$

$$q4 = \cos^{-1} \left(\frac{l05^2 - z3^2 - z4^2}{2 \cdot z3 \cdot z4} \right) \quad (5)$$

$$q5 = \text{atan2}(-r11 \cdot \sin(q1) \sin(q2) + r21 \cdot \cos(q2) \sin(q1) - r31 \cdot \cos(q1), r11 \cdot \cos(q2) + r21 \cdot \sin(q2)) - q3 - q4) \quad (6)$$

$$q6 = \cos^{-1} \left(\frac{l06yz^2 - l05yz^2 - z6^2}{2 \cdot l05yz \cdot z6} \right) \quad (7)$$

Equations (2-7) shows solutions for inverse kinematics problem for 6 DoF robot with spherical hip.

3.2.2 Numerical Solution

The inverse kinematics problem in the general case is the searching for the solution of a set of nonlinear algebraic equations. Most popular methods are the iterative ones. The most common method is the Newton-Raphson method, that can be found in (Jazar, 2010).

Before solving inverse kinematics with numerical method it necessary to find Jacobian of the robot.

The time derivative of the kinematics equations yields the robot Jacobian, which defines the joint contribution to the linear and angular velocity of the end-effector. Jacobian matrix has the size of $6 \times N$, where N number of DoF. It consists of two parts: Translational and Rotational. Jacobian for left leg:

$$J_{ee}(q) = \begin{bmatrix} J_v(q) \\ J_\omega(q) \end{bmatrix} \quad (8)$$

where $J_v(q)$ – translational part; $J_\omega(q)$ – rotational part.

Jacobian can be computed as the time derivative of forward kinematics equations, with skew theory, or as numerical derivatives. In this work, numerical derivatives were used.

$$TF = T_0 * [T(k-1)(q, \pi) * H(\pi_k) * T(k+1)(q, \pi)] * T_7 \quad (9)$$

$$T'_k = T_0 * [T(k-1)(q, \pi) * H'(\pi_k) * T(k+1)(q, \pi)] * T_7 \quad (10)$$

where $T(q, \pi)$ - the transformation matrices on the left and right sides of the currently considered parameter π_k , $H'(\pi_k)$ is the differential transformation matrix.

Elements of Jacobian will be equal to:

$$J_{\pi,k} = \begin{bmatrix} T'_{k, (1,4)} \\ T'_{k, (2,4)} \\ T'_{k, (3,4)} \\ [T'_k * TF^{-1}]_{(3,2)} \\ [T'_k * TF^{-1}]_{(1,3)} \\ [T'_k * TF^{-1}]_{(2,1)} \end{bmatrix} \quad (11)$$

There are numerous ways how to use Jacobian, but one of the most popular ones are pseudoinverse method and damped least square (DLS) method. The pseudoinverse method is widely discussed in the literature, but it often performs poorly because of instability near singularities. The damped least square method has better performance (Buss, 2004). Both of these methods were implemented and compared.

3.2.3 Hybrid Solution

In the proposed robot configuration hip joint is not spherical since the first three axes do not intersect at one point that means that previously described analytical solution cannot be used. Thus, numerical solution in this case shows non constant efficiency.

In order to improve numerical method efficiency a hybrid approach from (Cisneros Limón et al., 2013) is used. It consists of two phases. Phase one is to obtain approximate solution, since similar robot configuration with spherical hip joint is very close to our robot configuration. Phase two – use this approximate solution as initial for numerical method. It allows to greatly reduce the number of iterations.

The hybrid algorithm of inverse kinematics:

1. Set the initial counter $i = 0$.
2. Find $q(0)$ by using analytical solution of similar robot.
3. Calculate the residue $\delta T(q(i)) = J(q(i))\delta q(i)$. If every element of $T(q(i))$ or its norm $\|T(q(i))\|$ is less than a tolerance, $\|T(q(i))\| < \epsilon$ then terminate the iteration. The $q(i)$ is the desired solution.
4. Calculate $q(i+1)$ with pseudoinverse or DLS or any other technique.
5. Set $i = i + 1$ and return to step 3.

The performance of the hybrid and numerical algorithm was compared in order to evaluate its efficiency. The main evaluation parameters are (1) the number of iterations, which is needed to find a desired precision and orientation, and (2) the mean time required for computing this solution.

This evaluation was carried out over a data set consisting of 750 points along gait trajectory. Desired accuracy for numerical algorithm is equal to 10^{-6} m. Desired end effector position in X, Y, Z coordinates is shown in Figure 9a - 9c, whereas achieved joint angles is shown in Figure 9d. The results of the evaluation are shown in Table 5.

Table 5: Performance comparison of inverse kinematics algorithms.

Indicator	Iterations, ms	Execution time, ms
Analytical	1	0.04
Hybrid DLS	4	0.24
Numerical DLS	104	4.46
Numerical pseudoinverse	205	14.24

Hybrid solution is up to 20x faster than numerical DLS. It also has 100% cover rate, which means that all points of the test set (inside workspace) were reached. This algorithm allows real-time calculation with 50 Hz control loop, which is maximum for used robot.

3.3 Workspace Analysis

The workspace of a manipulator is defined as the volume of space, which the end-effector can reach. Two different definitions of workspace are usually used. A reachable workspace is the volume of space within which every point can be reached by the end effector in at least one orientation. A dexterous workspace is the volume of space within which every point can be reached by the end effector in all possible orientations. The dexterous workspace is a subset of reachable workspace (Jazar, 2010; Siciliano and Khatib, 2008).

According to robot task - forward walking on the flat surface, only inclusive orientation workspace is needed. In this case end-effector orientation locked to 0 deg. in roll, pitch and yaw. The workspace was calculated for different left foot positions relative to the torso coordinate Z: 0.325, 0.35, 0.375, and 0.43 meters (Figure 3). As a performance index for workspace Jacobean condition number was chosen. Condition number shows general accuracy, dexterity of the robot, closeness to singularity.

Since the robot configuration is a 6R serial chain for one leg, workspace is limited by serial singularity and mechanical joint limits. Serial singularity can be identified by low condition number near it. The mechanical joints limit appears as an unreachable area near the Y axis zero position (Hip joint limits) see Figure 4a, 4b, 4c and as an ellipse inside the workspace at small torso height (Knee joint limit) see Figure 4a, 4b.

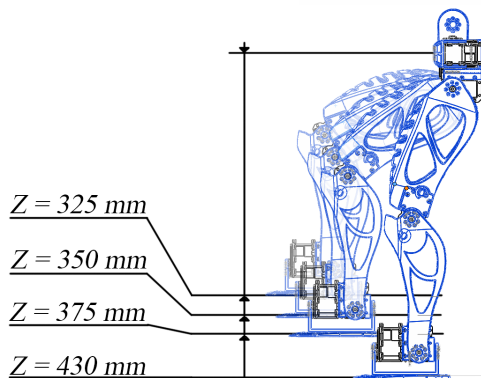


Figure 3: Foot positions relative to the torso coordinate Z.

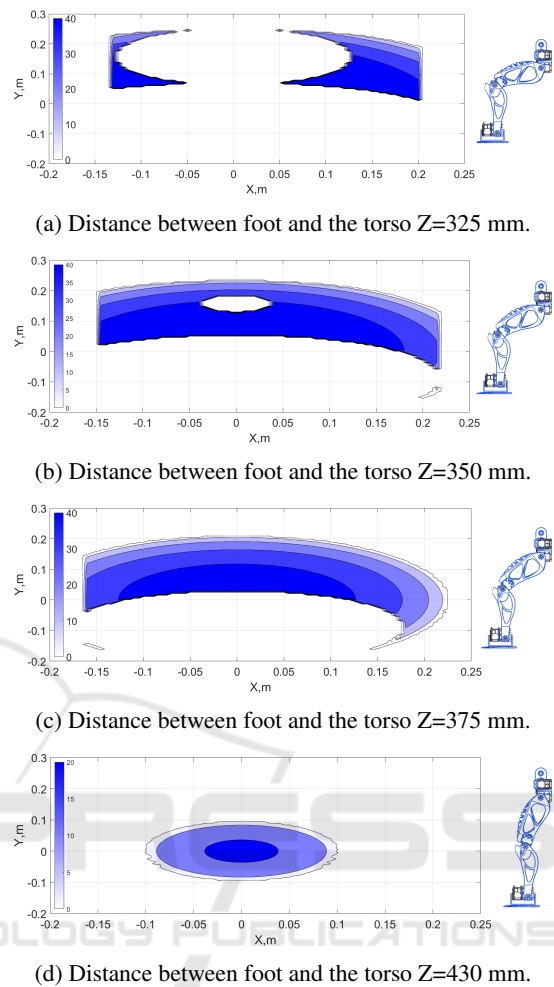


Figure 4: Achievable foot location and condition number with example configuration.

4 STIFFNESS ANALYSIS

In real life robot mechanical components (both joints and links) are not perfectly rigid, so the foot and torso position can differ from the expected one under the load induced by robot link weights. So if we need an accurate robot location and stable locomotion, we need to calculate these deflections and possibly to compensate them. This can be done by developing and analyzing robot stiffness model. This stiffness model can be obtained using Virtual Joint Method (VJM) (Pashkevich et al., 2011). According to this method non-rigid manipulator links can be represented as pair of rigid link and 6 DoF virtual spring and non-rigid actuators as perfect actuator and 1 DoF virtual spring describing its elasticity.

In practice, the end-effector position (foot or/and torso position) can be found from the extended geo-

metric model as

$$t = g(q, \theta) \quad (12)$$

where q is the vector of actuator coordinates $q = (q_1, q_2, \dots, q_n)^T$ and θ the vector of virtual joint coordinates $\theta = (\theta_1, \theta_2, \dots, \theta_m)^T$. Since the link weights are the main source of deflections in anthropomorphic robots, it should be also considered in the model. External load caused by weight of the links can be represented as forces acting in the node-points corresponding to virtual spring locations. In the simplified model used in this paper these virtual springs take into account both link and actuator compliances. By applying principle of virtual work, the static equilibrium of corresponding static system can be founded as (Klimchik et al., 2014)

$$J_{\theta}^{(G)T} \cdot G + J_{\theta}^{(F)T} \cdot F = K_{\theta} \cdot \theta \quad (13)$$

where the matrix $J_{\theta}^{(G)} = [J_{\theta}^{(1)T}, \dots, J_{\theta}^{(n)T}]^T$ aggregates partial Jacobians from the robot base to corresponding node point with gravity load, $J_{\theta}^{(F)}$ is the Jacobian from base of the robot to end-effector with external load, the vector G aggregates forces applied in the internal nodes (caused by gravity), F is vector of external load applied to the end-effector and $K_{\theta} = \text{diag}(K_{\theta_1}, \dots, K_{\theta_n})$ diagonal matrix with stiffness of all virtual springs. Desired static equilibrium configuration can be found using iterative algorithm (Klimchik et al., 2014).

$$\begin{aligned} F_{i+1} &= (J_{\theta}^{(F)} \cdot K_{\theta}^{-1} \cdot J_{\theta}^{(F)T})^{-1} \cdot (t_{i+1} - g(q, \theta_i) + \\ & J_{\theta_i}^{(F)} \cdot \theta_i - J_{\theta}^{(F)} \cdot K_{\theta}^{-1} \cdot J_{\theta}^{(G)T} \cdot G_i) \\ \theta_{i+1} &= K_{\theta}^{-1} (J_{\theta}^{(G)T} \cdot G_i + J_{\theta}^{(F)T} \cdot F_{i+1}) \end{aligned} \quad (14)$$

and the Cartesian stiffness matrix K_C can be computed as follows

$$\begin{bmatrix} K_C & * \\ * & * \end{bmatrix} = \begin{bmatrix} J_{\theta} \cdot K_{\theta}^{-1} \cdot J_{\theta}^T & J_q \\ J_q & 0 \end{bmatrix}^{-1} \quad (15)$$

this allows us to obtain force-deflection relation

$$\Delta t = K_C^{-1} \cdot F \quad (16)$$

where Δt end-effector deflections, and estimate compliance errors caused by gravity forces.

For the considered humanoid robot the main source of elasticity is related to the motor and gearbox flexibility. So, for simplicity, all links are considered to be rigid while actuated joints are considered to be deformable. Friction forces are not taken into account. According to the VJM notation 1 DoF virtual springs will be added after each actuator.

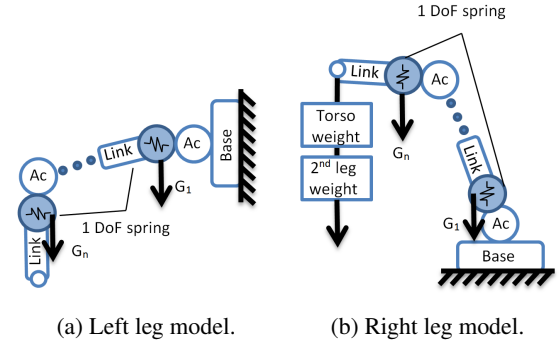


Figure 5: Robot VJM model.

For stiffness analysis of humanoid (similarly to kinematic and dynamic analyses) two walking phases should be addressed: single support phase (SSP) and dual support phase (DSP). In dual support stage both legs are on the ground. Assuming that there is no slip between surface and robot feet, it can be represented as parallel manipulator with two 6R serial chains. Deflections from external forces will only affect position of robot trunk and, assuming that deflections too small to move robot center of mass (CoM) out of support polygon, do not contribute to robot stability.

Most critical stage for bipedal robot where deflections can have a strong effect on stability is single support stage. In this stage one of the robot legs is swing and deflections caused by gravity force or/and external load can displace swaying leg closer to the ground or collide them. This undesired contact may lead the robot to fall. Robot VJM model in that stage can be introduced as two serial chains (Figure 5a and 5b). the first chain (Figure 5b) consist of 6 active joints and 6 virtual joints, base fixed to the surface. In addition to gravity forces G_n , there are external loadings caused by weight of upper body and swing leg. Second chain (Figure 5a) consists of 6 active joints and 6 virtual joints, base position can be found as end-effector position of first chain plus deflections in the end-effector of first chain. Second chain affected only by gravity forces G_n .

Total deflection can be calculated in 3 steps:

1. Calculate deflection for standing leg pelvis chain with gravity load and external load in end-effector that correspond to pelvis (upper body) mass + swing leg mass.
2. Calculate deflections for pelvis swing leg chain with swing leg gravity load.
3. Combine deflections from 2 chains.

Deflection magnitudes for different swing leg heights (presented in Figure 3) within the reachable workspace shown in Figure 6a, 6b, 6c, 6d. Right leg configuration (fixed on the floor) used for these

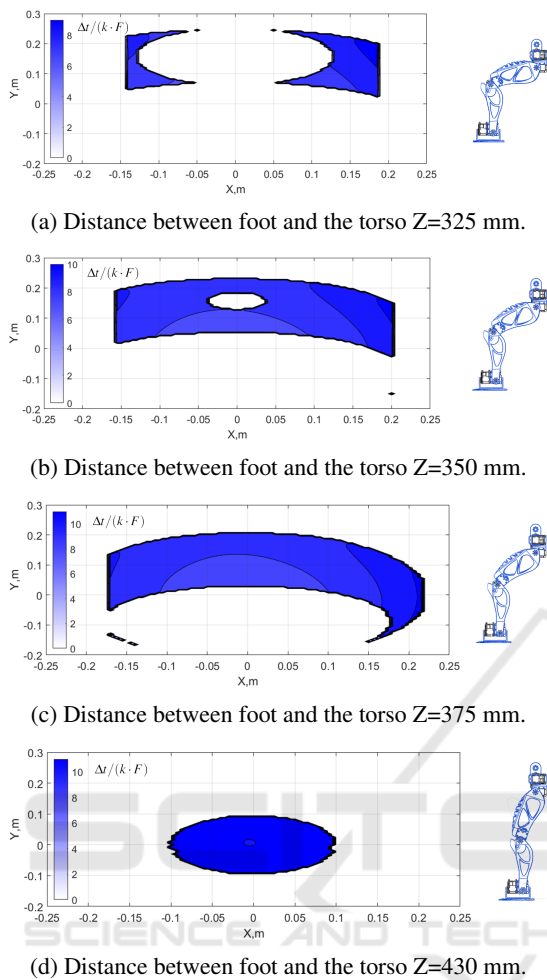


Figure 6: Deflections magnitude of the left foot for different swing leg height.

figures is static and all joint coordinates are equal to zero. It is shown that deflections are increasing near the border of the workspace. The minimal deflections can be achieved close to (0;0) point, but this configuration is not reachable by the swing leg for the heights less than 375 mm.

Deflection vector components for the swing leg high 375mm are shown in Figure 7a, 7b, 7c. Additional figures for other leg highs are presented in Appendix (Figures 13-16). Deflections in X and Y directions can be positive or negative, depending on the leg configuration. This behavior is explained by shifting robot center of mass. Deflections in Z direction have maximum magnitude and are the most critical ones, since they shift robot foot closer to the ground.

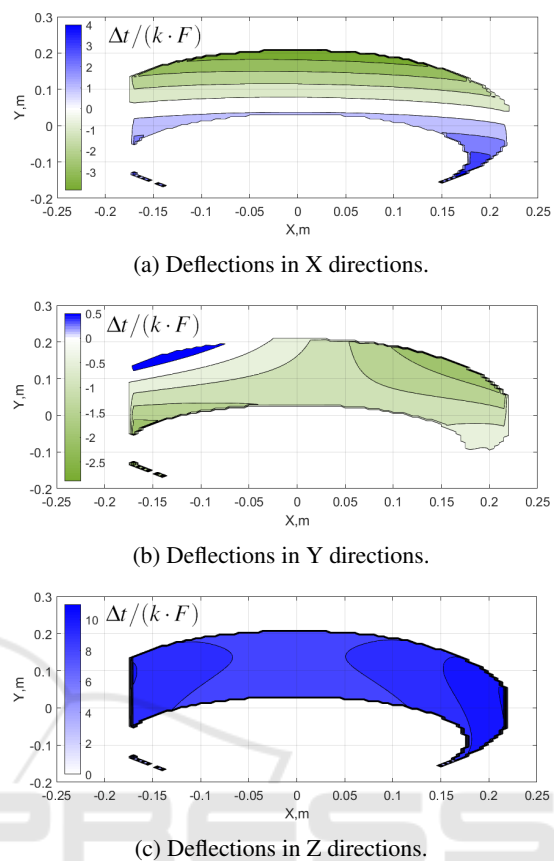


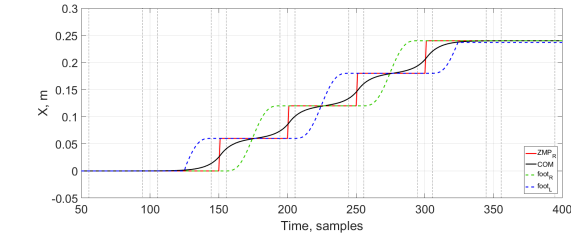
Figure 7: Deflection vector components for distance between foot and the torso $Z=375$ mm.

5 TRAJECTORY PLANNING

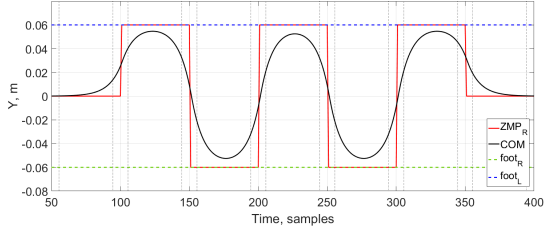
The biped walking pattern was obtained using Zero Moment Point (ZMP) preview control, proposed by (Kajita et al., 2003). ZMP preview control allows to obtain CoM trajectory based on ZMP-reference trajectory as it is shown in Figure 8a, 8b. With CoM trajectory and robot leg's end-effector trajectories it is possible to find joint angles with inverse kinematics described previously. Trajectory generated with this method assumes that robot links and joints are perfectly stiff. In order to include information about possible deflections to trajectory generation, external compensation technique is required.

The following algorithm for simple off-line compensation for SSP is used:

1. Generate trajectory for CoM using ZMP preview control.
2. Calculate deflections in each SSP for both legs for all points on trajectory.
3. Find new legs end effector coordinates as $p_{new} =$



(a) Robot motion in sagittal plane.



(b) Robot motion in lateral plane.

Figure 8: Walking pattern generated by preview control.

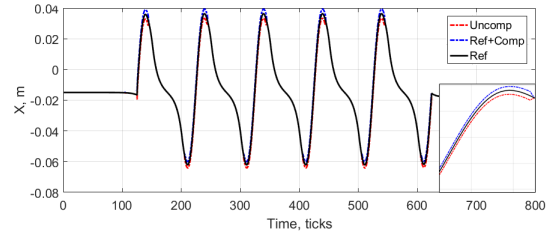
$$p - \Delta t.$$

4. Recalculate inverse kinematics for new trajectories.

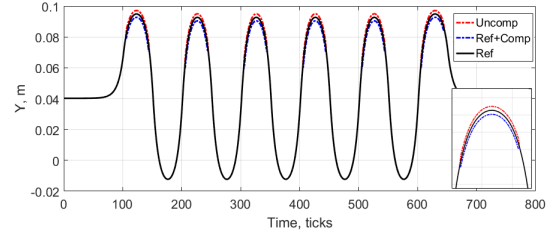
For simulation following walking pattern generation parameters were used:

- Step size - 6 cm
- CoM height - 43 cm
- Number of step phases = 15 (for demonstration)
- Control frequency - 50 Hz
- Leg lift - 5 cm
- Dual support phase - 20%.

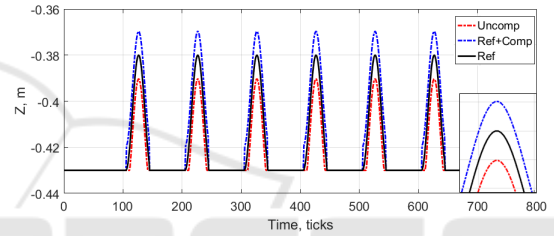
Ankle trajectories in X, Y, Z plane are shown in Figure 9a, 9b, 9c respectively. Deflections in X and Y planes are small compared to Z. Table 6 shows normalized position error value with and without compensation. High improvement factor can be explained by the linearity of the model. Joint trajectories with and without compensation are presented in Figure 9d. Knee, hip and ankle joints rotating around Y axis have the most essential changes due to compensation, since they correspond to movements of end-effector in Z direction, where deflections have maximal magnitude. Difference between reference and compensated control signal for left leg ankle shown in Figure 10. Since only the SSP is considered for compensation, error for intervals where the left leg placed on the ground are equal to zero. Lower amplitude of error in the first step can be explained by the fact that first step is actually a half-step.



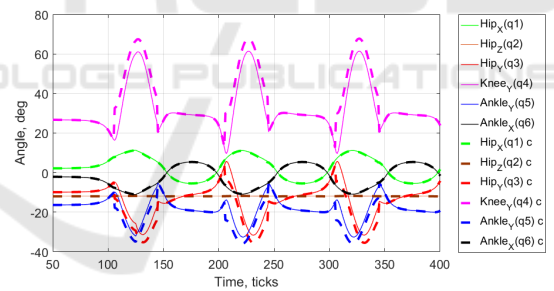
(a) Ankle position X.



(b) Ankle position Y.



(c) Ankle position Z.



(d) Joint angles.

Figure 9: reference and non-compensated spatio-temporal joint trajectories for robot gait.

Total stability improvement for the biped robot can be observed by looking at ZMP position and its position error compared to reference ZMP trajectory. Trajectories obtained from preview control (Figure 8a, 8b) were examined with the robot model in V-REP, after that ZMP trajectory were obtained from virtual sensors. Figure 11a, 11b present ZMP position in Y and X plane over time. ZMP position without compensation has a noticeable peak at the point where foot of the robot contacted with ground surface and because of deflections it's happen before DSP defined by the algorithm. This cause robot to stumble and move its ZMP closer to the edges of sup-

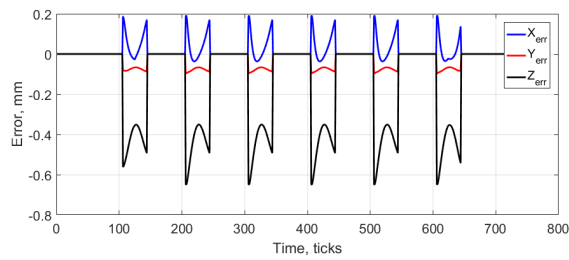
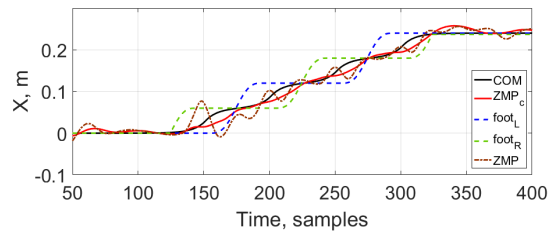
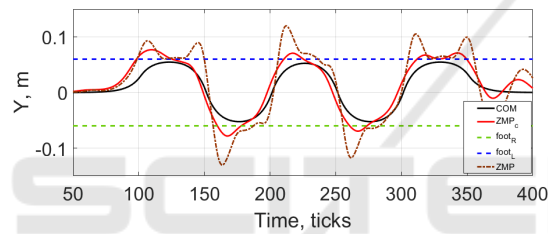


Figure 10: Error between reference and compensated trajectory for ankle position.



(a) Robot motion in sagittal plane.



(b) Robot motion in lateral plane.

Figure 11: Simulated robot walking trajectories with and without compensation in V-REP.

port polygon. Maximum amplitude of difference between compensated/non-compensated and reference ZMP position presented in Table 7. Figure 12 introduce ZMP position with and without compensation in XY plane (top view). Using compensation of deflections allowed to reduce error by 61% in X plane (forward movements) and by 73% in Y plane (side movements).

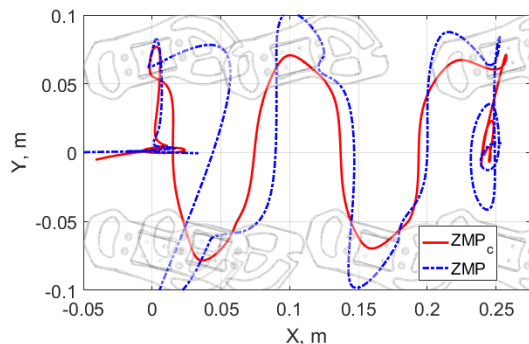


Figure 12: Simulated biped robot ZMP with and without compensation in XY plane.

Table 6: Maximum end-effector position errors.

	Error before compensation ($\Delta t / (k \cdot F)$)	Error after compensation ($\Delta t / (k \cdot F)$)	%
X	3.06	0.19	93.8
Y	2.22	0.09	95.9
Z	10.41	0.65	93.7

Table 7: Maximum ZMP errors compared to reference.

	Error before compensation (mm)	Error after compensation (mm)	%
X	51.62	20.04	61.2
Y	68.41	18.27	73.3

The simulated ZMP trajectory was also validated on the real 3D-printed robot prototype. During tests robot demonstrated stable walking capability with off-line generated joint trajectories.

6 DISCUSSION

Stiffness modeling for bipedal robots allow to reduce position error for the robot legs, especially in Z direction, that is critical for stable walking ability. In this work only the joint compliance was used, but it's possible to further improve stiffness model by implementing a link stiffness model in addition to joint model. This improved model will allow to increase error reduction depending on the robot structure (Klimchik et al., 2015). Link compliance is more valuable for full-size humanoid robots, where mass of the robot parts is relativity high. The robot used in this work has small size and low mass and link compliance could be ignored. But in the same time material (ABS - plastic) has quite low Young's modulus value and process (Fused deposition modeling) used for robot link creation will reduce total stiffness of the robot links. Further experiments required in order to understated how implementing of more complicated model will increase performance of walking motion. Another way of increasing error reduction is implementation of non-linear model that could further decrease error.

The current algorithm calculates deflection off-line. For humanoid robot that could constantly recalculates moving trajectory based on its environment on-line method should be implemented by computing possible deflection each control cycle or by using previously calculated patterns.

7 CONCLUSIONS

The main goal of this work was to design low-cost bipedal anthropomorphic robot, provide stiffness analysis and implement error compensation technique. The biped robot was designed based on open source Poppy Humanoid project with 10 DoF lower limbs, but with enhancing their mechanical structure and functionality with additional DoF at the ankle. The robot's lower body was modeled in V-REP simulator and prototyped using 3D printing technology. Despite increasing DoF relative to Poppy humanoid, we succeeded to reduce overall cost using hobby servomotors, inexpensive fabrication methods and cost-efficient electronics components. As far as the current robot design has a non-spherical hip joint, which does not allow to use an analytical solution for the inverse kinematics, we computed inverse kinematics using hybrid and numerical methods. Stiffness model of the robot was obtained using VJM for single support phase and main source of compliance in the robot joints. Integration of stiffness model into gait pattern generation algorithm allowed us to compensate deflections caused by link weights. These trajectories were examined both with the robot model in V-REP simulator and on the real 3D-printed lower body prototype. The results of experiments demonstrated stable walking capability of the designed Poppy-inspired humanoid with 12 DoF lower limbs.

Future work includes deep consideration of motion processes, creation and implementation of on-line trajectory generation and compensation, using stiffness model along with the variable stiffness actuators. For hardware part the main future tasks are to enhance and to produce lower limbs with a higher motion range, passive/active joints with spring support, and to design robots upper body.

ACKNOWLEDGEMENTS

This research has been supported by the grant of Russian Ministry of Education and Science 2017-14-576-0053-7882 and Innopolis University

REFERENCES

- Buss, S. R. (2004). Introduction to inverse kinematics with jacobian transpose, pseudoinverse and damped least squares methods. *IEEE Journal of Robotics and Automation*, 17(1-19):16.
- Cisneros Limón, R., Ibarra Zannatha, J. M., and Armada Rodriguez, M. A. (2013). Inverse kinematics of a humanoid robot with non-spherical hip: a hybrid algorithm approach. *International Journal of Advanced Robotic Systems*, 10:1–13.
- Craig, J. J. (2005). *Introduction to robotics: mechanics and control*, volume 3. Pearson Prentice Hall Upper Saddle River.
- Ferro, F. and Marchionni, L. (2014). Reem: A humanoid service robot. In *ROBOT2013: First Iberian Robotics Conference*, pages 521–525. Springer.
- Gouaillier, D., Hugel, V., Blazevic, P., Kilner, C., Monceaux, J., Lafourcade, P., Marnier, B., Serre, J., and Maisonnier, B. (2009). Mechatronic design of nao humanoid. In *Robotics and Automation, 2009. ICRA'09. IEEE International Conference on*, pages 769–774. IEEE.
- Ha, I., Tamura, Y., Asama, H., Han, J., and Hong, D. W. (2011). Development of open humanoid platform darwin-op. In *SICE Annual Conference (SICE), 2011 Proceedings of*, pages 2178–2181. IEEE.
- Jazar, R. N. (2010). *Theory of applied robotics: kinematics, dynamics, and control*. Springer Science & Business Media.
- Kajita, S., Kanehiro, F., Kaneko, K., Fujiwara, K., Harada, K., Yokoi, K., and Hirukawa, H. (2003). Biped walking pattern generation by using preview control of zero-moment point. In *Robotics and Automation, 2003. Proceedings. ICRA'03. IEEE International Conference on*, volume 2, pages 1620–1626. IEEE.
- Khusainov, R., Shimchik, I., Afanasyev, I., and Magid, E. (2015). Toward a human-like locomotion: Modelling dynamically stable locomotion of an anthropomorphic robot in simulink environment. In *Informatics in Control, Automation and Robotics (ICINCO), 2015 12th International Conference on*, volume 02, pages 141–148.
- Klimchik, A., Chablat, D., and Pashkevich, A. (2014). Stiffness modeling for perfect and non-perfect parallel manipulators under internal and external loadings. *Mechanism and Machine Theory*, 79:1–28.
- Klimchik, A., Furet, B., Caro, S., and Pashkevich, A. (2015). Identification of the manipulator stiffness model parameters in industrial environment. *Mechanism and Machine Theory*, 90:1–22.
- Lapeyre, M., N'Guyen, S., Le Falher, A., and Oudeyer, P.-Y. (2014). Rapid morphological exploration with the poppy humanoid platform. In *2014 IEEE-RAS International Conference on Humanoid Robots*, pages 959–966. IEEE.
- Lapeyre, M., Rouanet, P., and Oudeyer, P.-Y. (2013a). Poppy humanoid platform: Experimental evaluation of the role of a bio-inspired thigh shape. In *2013 13th IEEE-RAS International Conference on Humanoid Robots (Humanoids)*, pages 376–383. IEEE.
- Lapeyre, M., Rouanet, P., and Oudeyer, P.-Y. (2013b). The poppy humanoid robot: Leg design for biped locomotion. In *2013 IEEE/RSJ International Conference on Intelligent Robots and Systems*, pages 349–356. IEEE.
- Pashkevich, A., Klimchik, A., and Chablat, D. (2011). Enhanced stiffness modeling of manipulators with

passive joints. *Mechanism and machine theory*, 46(5):662–679.

- Peiper, D. L. (1968). The kinematics of manipulators under computer control. Technical report, DTIC Document.
- Rohmer, E., Singh, S. P., and Freese, M. (2013). V-rep: A versatile and scalable robot simulation framework. In *2013 IEEE/RSJ International Conference on Intelligent Robots and Systems*, pages 1321–1326. IEEE.
- Sakagami, Y., Watanabe, R., Aoyama, C., Matsunaga, S., Higaki, N., and Fujimura, K. (2002). The intelligent asimo: System overview and integration. In *Intelligent Robots and Systems, 2002. IEEE/RSJ International Conference on*, volume 3, pages 2478–2483. IEEE.
- Siciliano, B. and Khatib, O. (2008). *Springer handbook of robotics*. Springer Science & Business Media.
- Yamaguchi, J., Soga, E., Inoue, S., and Takanishi, A. (1999). Development of a bipedal humanoid robot-control method of whole body cooperative dynamic biped walking. In *Robotics and Automation, 1999. Proceedings. 1999 IEEE International Conference on*, volume 1, pages 368–374. IEEE.

APPENDIX

Analytical Solution for Inverse Kinematic

In the sagittal plane (Figure 2b) we consider lengths Z_3 , Z_4 and l_{05} .

The position of the ankle T_x , T_y , T_z can be obtained from the inverse matrix of $T6 * T7$ (1).

$$T1 * T2 * T3 * T4 * T5 = TF * (T6 * T7)^{-1} = \begin{bmatrix} * & * & * & T_x + z_6 \cdot r_{13} \\ * & * & * & T_y + z_6 \cdot r_{23} \\ * & * & * & T_z + z_6 \cdot r_{33} \\ 0 & 0 & 0 & 1 \end{bmatrix} \quad (17)$$

Then find distance l_{05} as

$$(l_{05})^2 = (T_x + z_6 \cdot r_{13})^2 + (T_y + z_6 \cdot r_{23})^2 + (T_z + z_6 \cdot r_{33})^2 \quad (18)$$

The knee angle $q4$ can be calculated from the law of cosines

$$q4 = \cos^{-1} \left(\frac{l_{05}^2 - z_3^2 - z_4^2}{2 \cdot z_3 \cdot z_4} \right) \quad (19)$$

Lengths l_{06yz} and l_{05yz} can be found in the frontal plane (Figure 2a).

$$l_{06yz} = \sqrt{(TF^{-1}(2,4))^2 + (TF^{-1}(3,4))^2} \quad (20)$$

$$l_{05yz} = \sqrt{(TF^{-1}(2,4))^2 + (TF^{-1}(3,4) - z_6)^2} \quad (21)$$

The ankle roll angle can be calculated by the law of cosine

$$q6 = \cos^{-1} \left(\frac{l_{06yz}^2 - l_{05yz}^2 - z_6^2}{2 \cdot l_{05yz} \cdot z_6} \right) \quad (22)$$

$$T1 * T2 * T3 * T4 = TF * (T5 * T6 * T7)^{-1} \quad (23)$$

Find $q1$ and $q2$ from (23), by comparing right hand side (RHS) and left hand side (LHS) equations.

If we inverse $T1 * T2$, $T6 * T7$ and multiply them with TF

$$T3 * T4 * T5 = (T1 * T2)^{-1} * TF * (T6 * T7)^{-1} \quad (24)$$

Then RHS and LHS equations will be:

$$RHS = \begin{bmatrix} * & * & * & A \\ * & * & * & B \\ * & * & * & * \\ 0 & 0 & 0 & 1 \end{bmatrix} \quad (25)$$

where

$$A = -T_x \cdot \sin(q2) \sin(q1) + T_y \cdot \cos(q2) \sin(q1) - T_z \cdot \cos(q1) - z_6(r_{13} \cdot \sin(q1) \sin(q2) - r_{23} \cdot \cos(q2) \sin(q1) + r_{33} \cdot \cos(q1)) \quad (26)$$

$$B = -T_x \cdot \cos(q2) - T_y \cdot \sin(q2) - z_6(r_{13} \cdot \cos(q2) + r_{23} \cdot \sin(q2)) \quad (27)$$

$$LHS = \begin{bmatrix} * & * & * & C \\ * & * & * & D \\ * & * & * & * \\ 0 & 0 & 0 & 1 \end{bmatrix} \quad (28)$$

where

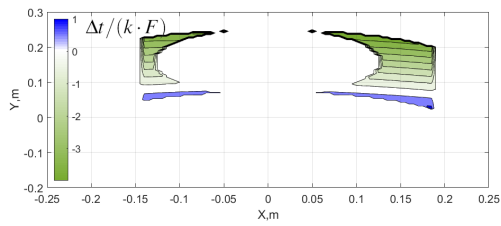
$$C = (z_3 + z_4 \cdot \cos(q4)) \cos(q3) - z_4 \cdot \sin(q4) \sin(q3) \quad (29)$$

$$D = z_4 \cdot \sin(q4) \cos(q3) + (z_3 + z_4 \cdot \cos(q4)) \sin(q3) \quad (30)$$

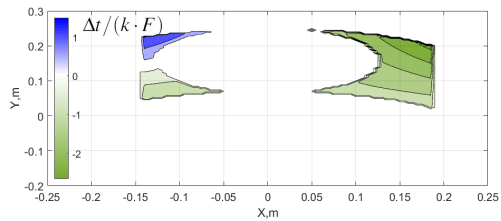
Solve it for $q3$ and then find $q5$ from known $q3$ and $q4$. Final equations for 6 DoF leg presented in section 3.2.1

Deflections Maps for Biped Robot

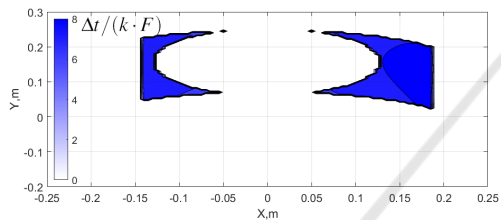
Figures 13-16 shows X, Y, Z deflection vector components for the left leg height is presented in Figure 3.



(a) Deflections in X directions.

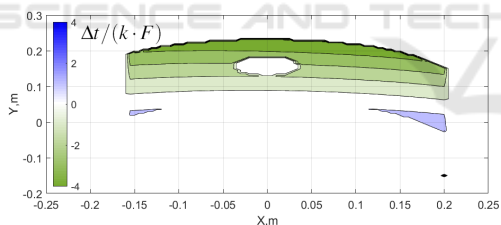


(b) Deflections in Y directions.

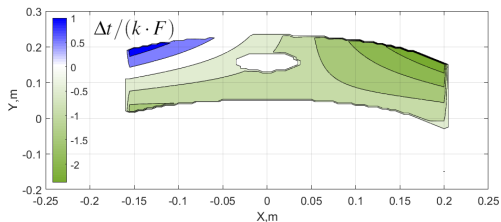


(c) Deflections in Z directions.

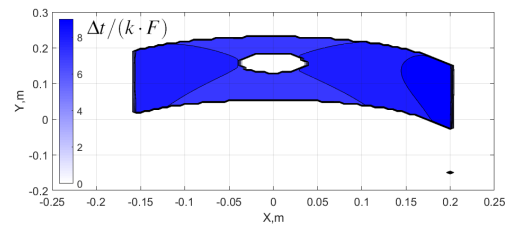
Figure 13: Deflection vector components for distance between foot and the torso $Z=325$ mm.



(a) Deflections in X directions.

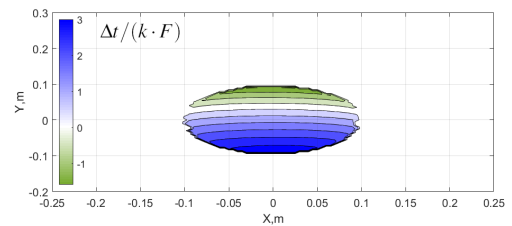


(b) Deflections in Y directions.

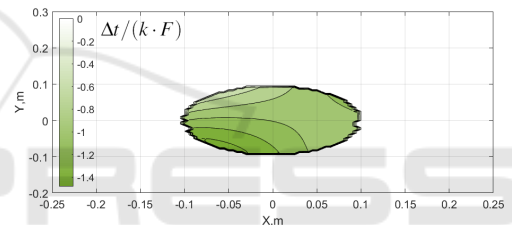


(c) Deflections in Z directions.

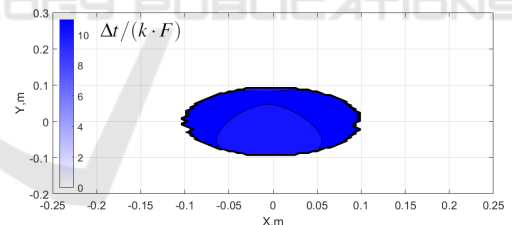
Figure 14: Deflection vector components for distance between foot and the torso $Z=350$ mm.



(a) Deflections in X directions.

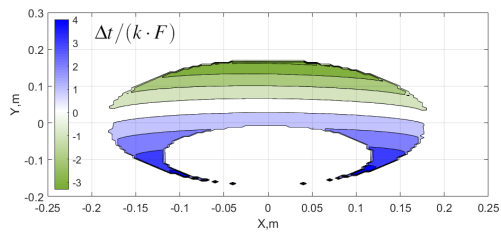


(b) Deflections in Y directions.

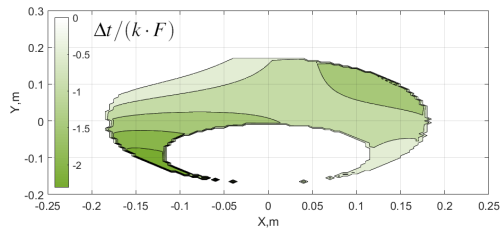


(c) Deflections in Z directions.

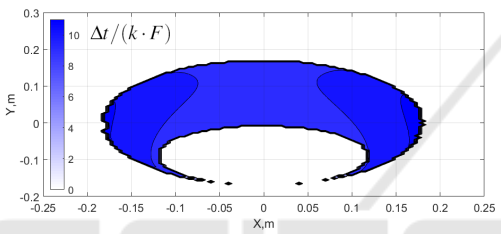
Figure 15: Deflection vector components for distance between foot and the torso $Z=430$ mm.



(a) Deflections in X directions.



(b) Deflections in Y directions.



(c) Deflections in Z directions.

Figure 16: Deflection vector components for distance between foot and the torso $Z=400$ mm.